Several Methods Used In Observational Astrophysics

Marcel Haas, Sebastiaan Keek and Hariëtte Freling

Summary

In this practicum session we will emphasize three different things you encounter in observational astrophysics. In the first part Fourier Transforms and their use in astronomy. Secondly we we will see how it is possible to detect a pulsar signal from a background dominated radiation field with use of the Fast Fourier Transform. The last project emphasizes the Signal to Noise Ratio and how it is used in designing instruments.

1 Wave packets and Fourier Transforms

1.1 Fourier Transforms

We derive an expression for the Fourier transform of a spectral line.

$$H(\omega) = \frac{1}{\sqrt{2\pi}\sigma_{\omega_0}} e^{-\frac{1}{2}(\frac{\omega-\omega_0}{\sigma_{\omega_0}})^2} \quad (1)$$

$$h(t) = \frac{1}{2\pi}\int_{-\infty}^{\infty} H(\omega)e^{i\omega t}d\omega \quad (2)$$

$$h(t) = -\frac{e^{-\frac{1}{2\sigma^2}}}{2\pi\sqrt{2\pi}\sigma}\int_{-\infty}^{\infty} e^{-(\omega-\omega_0)^2+i\omega t}dt \quad (3)$$

$$\omega = W + \omega_0 \leftrightarrow W = \omega - \omega_0 \quad (4)$$

$$h(t) = K\int_{-\infty}^{\infty} e^{-W^2+i(W+\omega_0)t}dW \quad (5)$$

$$K = -\frac{e^{-\frac{1}{2\sigma^2}}}{2\pi\sqrt{2\pi}\sigma} \quad (6)$$

$$h(t) = Ke^{i\omega_0 t}\int_{-\infty}^{\infty} e^{iWt-W^2}dW \quad (7)$$

$$h(t) = Ke^{i\omega_0 t}\sqrt{\pi}e^{-\frac{t^2}{4}} \quad (8)$$

$$h(t) = \frac{e^{-\frac{1}{2}(\frac{t^2}{2}+\frac{1}{\sigma^2})}}{\sqrt{8}\pi\sigma_{\omega_0}}e^{i\omega_0 t} \quad (9)$$

If we plot the wave packets and their Fourier transforms for various standard deviations, we obtain the following plots:

If the wave packet becomes smaller, its Fourier transform gets wider and vice versa.

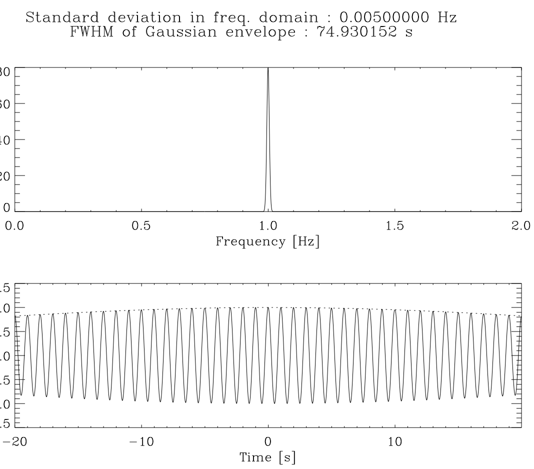

Figure 1: The wave packet and its Fourier transform for $\sigma_{\omega_0} = 0.005$

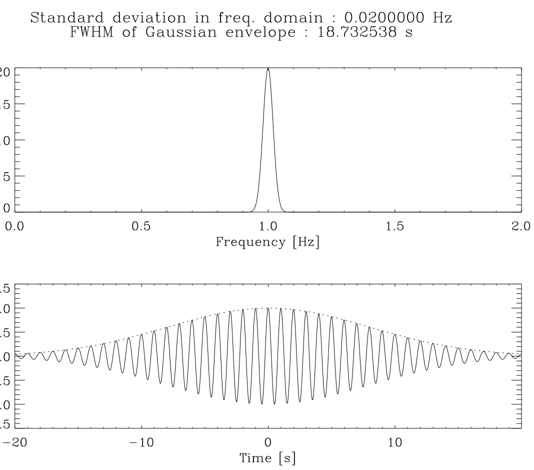

Figure 2: The wave packet and its Fourier transform for $\sigma_{\omega_0} = 0.02$

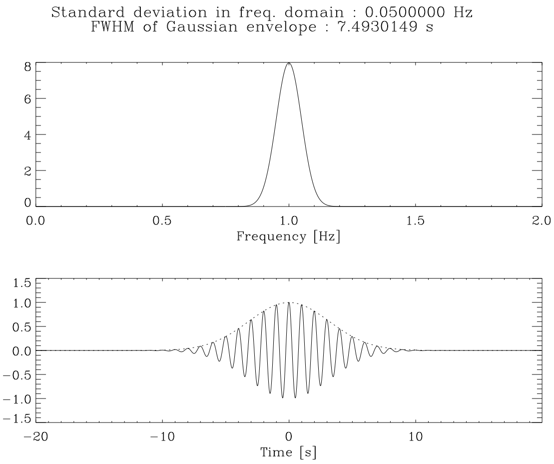

Figure 3: The wave packet and its Fourier transform for $\sigma_{\omega_0} = 0.05$

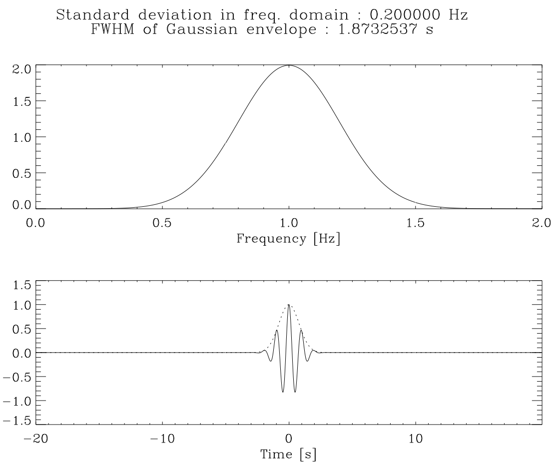

Figure 4: The wave packet and its Fourier transform for $\sigma_{\omega_0} = 0.2$

1.2 Interference

Now we will consider two wave packets and let them interfere. We use the same wave packets as before, each time with a different time shift. We will become destructive as well as constructive interference, depending on the mutual time shifts, where tyhe wave packets overlap.

Here are several plots:

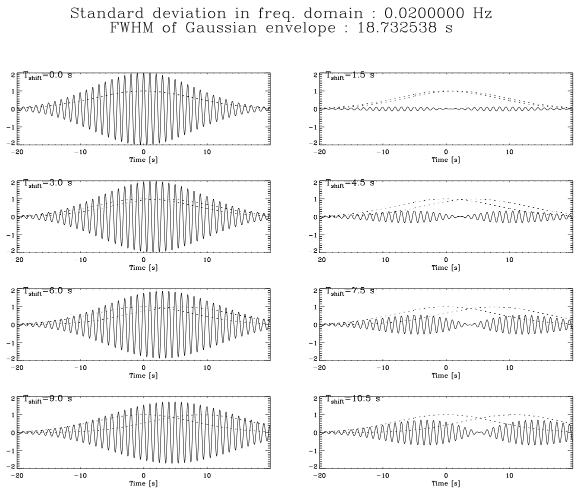

Figure 5: Several wave packets interfering at different time shifts.

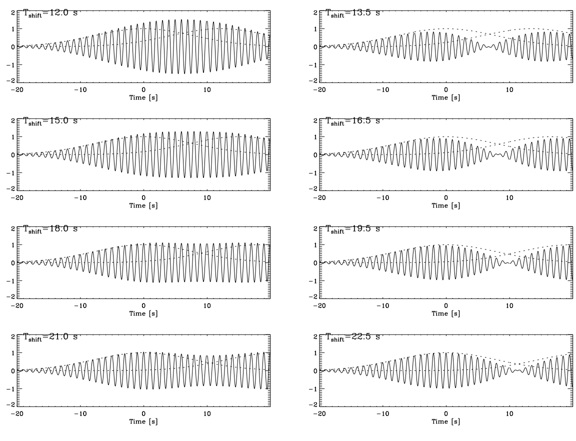

Figure 6: Several wave packets interfering at different time shifts.

It can easily be seen that interference only is possible on time scales of order of the interference time. The fluctuations in the interference pattern are of the same order of the pattern itself.

1.3 Monochromatic Waves

We can generalize the interference pattern to n wave packets, to generate a so-called quasi-monochromatic waves. To illustrate this we use $n = 400$ and we make plots of the interference patterns for different standard deviations.

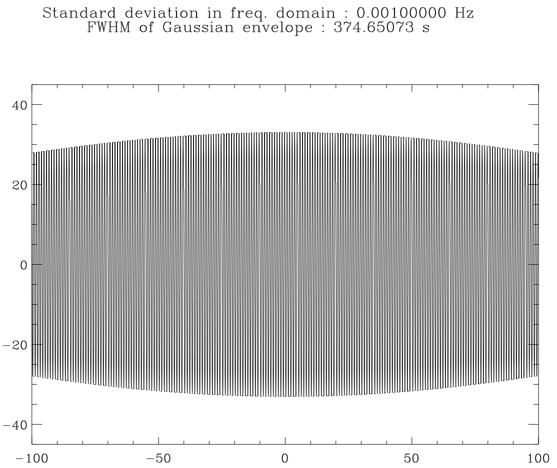

Figure 7: The interference pattern for a superposition of 400 waves and a standard deviation of 0.001 Hz

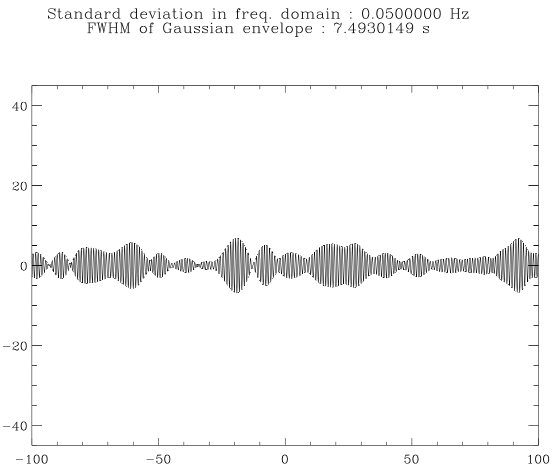

Figure 8: The interference pattern for a superposition of 400 waves and a standard deviation of 0.05 Hz

If we describe the patterns like $E(t) = E_0(t)\cos 2\pi\overline{\nu}t + \phi(t)$, where $\overline{\nu}$ is the frequency of the carrier wave, $\phi(t)$ a time-dependent phase angle and $E_0(t)$ the slowly varying time dependent amplitude modulation function. The typical time scale of the latter is much higher than the coherence time.

If in an interference experiment the separation between the pinhole is distorted by more than two times the coherence length there will be no interference.

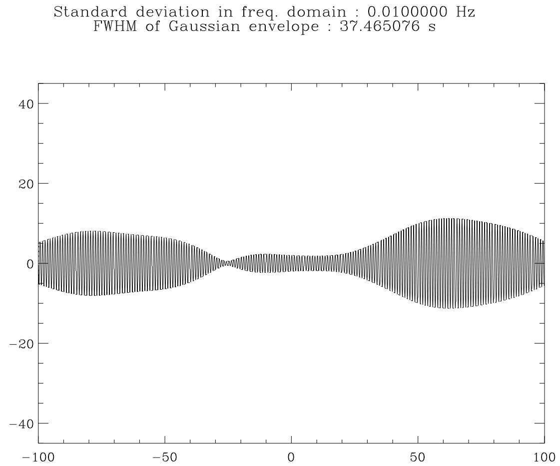

Figure 9: The interference pattern for a superposition of 400 waves and a standard deviation of 0.01 Hz

1.4 Krypton-86

Finally we use the results obtained before on one of the most coherent non-laser lines, ^{86}Kr at 605.8 nm, and of a He-Ne-laser line at 632.8 nm.

The width $\Delta\lambda$ of the orange Krypton line is 0.00055 nm, so the line frequency is 4.9510^{14} Hz, $\Delta\nu = 8.9910^{8}$ Hz. The frequency stability, defined as $\frac{\nu}{\Delta\nu} = 550727$ and the coherence length is 33 cm.

For a helium-neon laser with a frequency stabilty of 2 parts in 10^{10}, the coherence length at $\lambda = 632.8$ nm is 3.164 km!

2 Pulsar Detection

2.1 Detecting the Signal

We use a list of simulated pulsar counts, with background. The pulsar counts are drawn from a single Gaussian peak characterized by a known FWHM. For given simulation set 1, we generate the timestamp sample composed of both background and pulsar counts. We convert this individual photon timestamps into a count rate array adopting a certain sampling frequency in order to use the Fourier transform concept.

If we make a time plot of the count rate versus time, we obtain Figure 10. It is obvious that the signal is not easily detected with the eye.

Using an IDL procedure we perform a discrete Fourier transform of the count rate. Internally in this procedure the average count rate is subtracted from the actual count rate. The result is Fourier transformed. The result of this transformation is a power density spectrum versus signal frequency, which can be seen in Figure 11. In this plot the signal is easily recognized. We determine the frequency of the

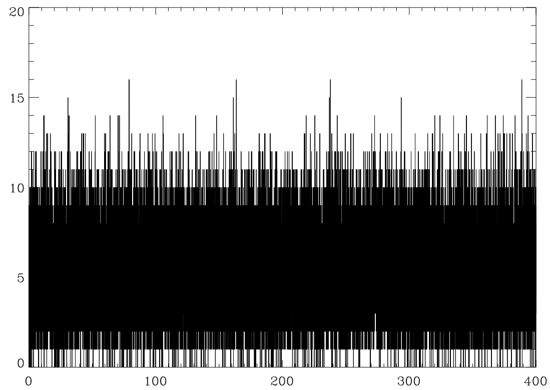

Figure 10: The count rate versus time.

pulsed signal to be 5 Hz, as can be seen at the horizontal axis.

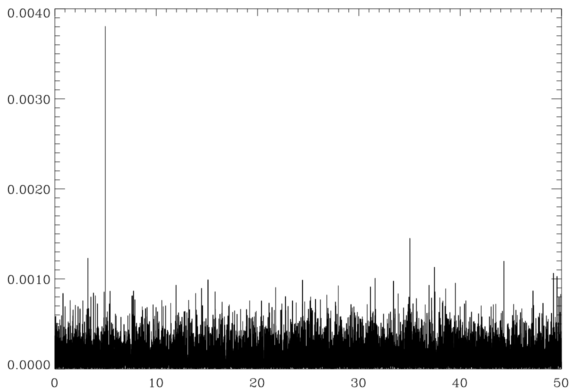

Figure 11: The power density spectrum versus signal frequency.

2.2 The Properties of the Signal

Now we have found the signal of the pulsar in a background dominated environment, we want to know the properties of the signal. First a phase histogram of the timestamp series is made (by pulse phase folding the series with the found frequency): Figure 12. The result is a pulse profile of the pulsar atop of a flat background distribution. The effective width, or duty cycle, of the pulse is 0.4. That's exactly the FWHM of the simulated pulsar.

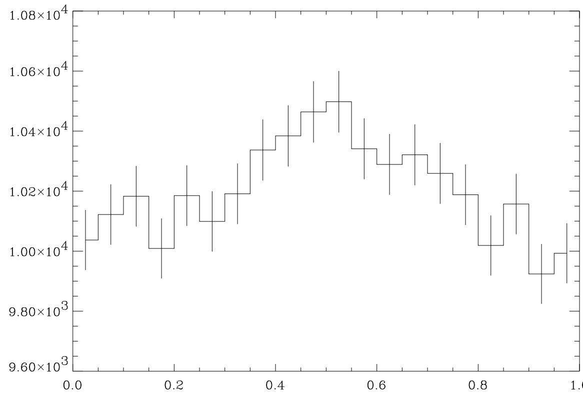

Figure 12: Phase histogram of the timestamp series.

2.3 Comparison with another Pulsar Simulation

Another pulsar simulation is made. The difference between the sets will appear from the plots. Exactly the same plots are made of this example.

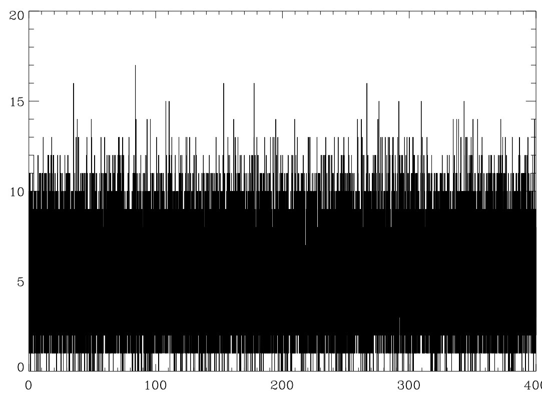

Figure 13: The count rate versus time of the second simulated pulsar.

Again, in the signal (Figure 13) nothing is to be seen. When we make the power spectrum (Figure 14) we can see more than one peak. The explanation for that is that the FWHM of the Gaussian is smaller than in the first set. In order to obtain such a signal you need more higher harmonics in the Fourier spectrum. Thats why there are clear peaks at two, three and four times the signal frequency. If we made the FWHM even smaller, more and more peaks will appear in the Fourier spectrum.

In Figure 15 the phase histogram of this simulated pulsar is plotted. From this plot it is clear that the FWHM is indeed smaller (0.2 instead of 0.4)

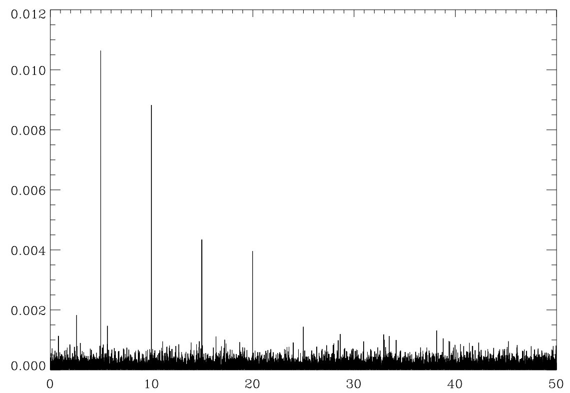

Figure 14: The power density spectrum versus signal frequency of the second simulated pulsar.

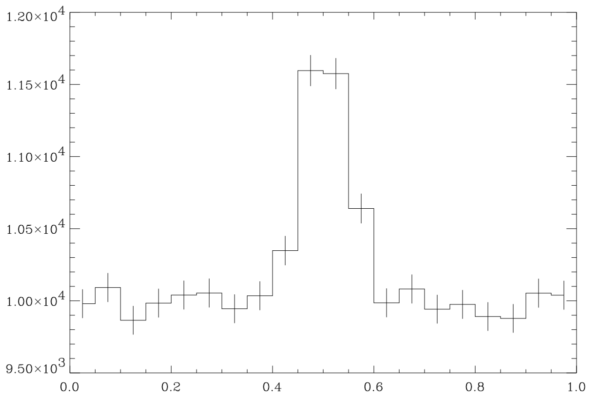

Figure 15: Phase histogram of the timestamp series of the second simulated pulsar.

2.4 The Effect of the Sampling Frequency

In the simulations a sampling frequency of 100 Hz was used. The found signal turned out to have a frequency much lower than that. If the sampling frequency was chosen smaller than the hypothetical pulsar frequency we would have counted more than one pulse in the time of one sample. The result would be that in every bin there is at least one photon of the source counted. The frequency cannot be determined.

3 Signal to Noise Ratio Dependence on Background, Number of Pulsed Counts and Duty Cycle

Now we have obtained the pulse phase distribution of the signal we can study in more detail the dependencies of the S/N-ratio on the pulsed signal strength (the number of pulsed counts), background and width of the pulse.

In our case the S/N-ratio (the ratio of pulsed excess counts and error in pulsed excess counts) can be determined from:

$$S/N = \frac{N_P - (\Delta_{on}/(1-\Delta_{on})) \cdot N_U}{\sqrt{N_P - (\Delta_{on}/(1-\Delta_{on}))^2 \cdot N_U}} \qquad (10)$$

N_P represents the total number of counts in the pulsed phase interval, while N_U is the total number of counts in the unpulsed interval. The width of the pulsed interval is given by Δ_{on}.

3.1 Pulsar Simulation

We generated a simulated set of pulse phases using N_{pulsar} = 500 pulsed counts, N_{bg} = 20000 background counts and a pulse FWHM of 0.1. A pulse histogram of the pulsed signal is shown in Figure 16. In this plot the FWHM of the signal is fixed, the number of pulsed counts goes from 500 to 2000 in steps of 250. The signal to noise ratio as a function of input pulsed counts is plotted in Figure 17. It is clear that this ratio decreases as a function of input pulsed counts.

Now we let the number of pulsed counts as well as the FWHM fixed and we let the number of background counts vary from 20000, 45000, 80000, 125000, 180000, 245000 up to and including 320000. The Phase histograms are plotted in Figure 18.

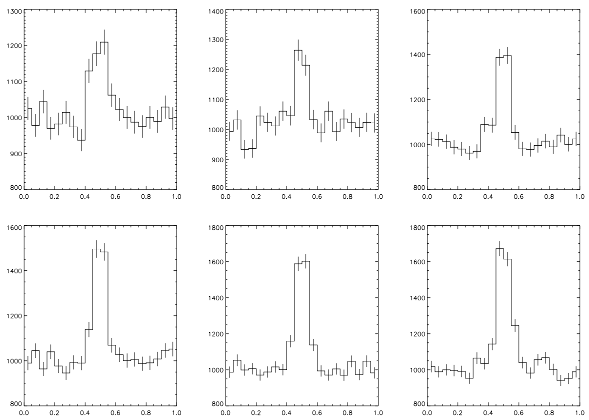

Figure 16: Phase histograms of a simulated pulsar with the FWHM fixed and the number of pulsed counts increasing.

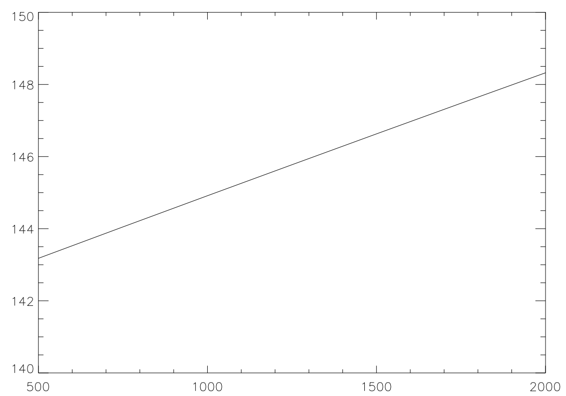

Figure 17: The signal to noise ratio as a function of input pulsed counts.

Again the signal to noise ratio is plotted as a function of the number of background counts, as can be seen in Figure 19.

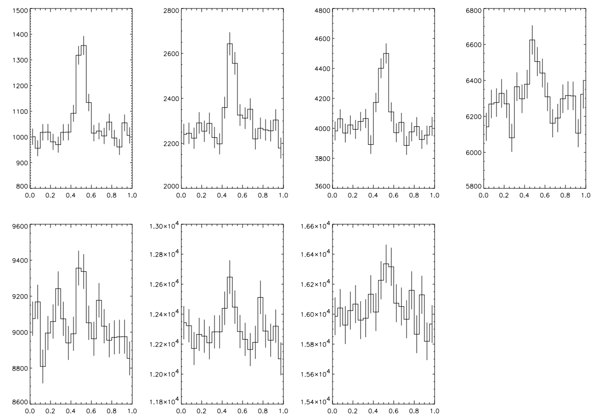

Figure 18: Phase histograms with FWHM and pulsed counts fixed, with increasing background counts.

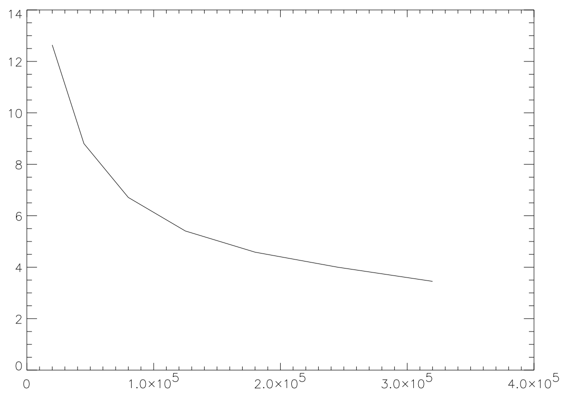

Figure 19: The signal to noise ratio as a function of background counts.

Finally we put the number of pulsed counts and the number of background counts fixed and let the FWHM vary from 0.1 up to 0.3 in steps of 0.05. The result can be seen in Figure 20. And also a plot of the S/N-ratio dependence is made in Figure 21.

All the plots of the signal to noise ratio are means of 100 simulations to make the resulting plot more general. From these plots it is obvious that the signal to noise ratio is getting higher (and hence better) for a higher number of pulsed counts (linear). It gets smaller when the number of background counts is higher (square root). The S/N-ratio gets smaller of the FWHM of the signal is smaller (more or less linear).

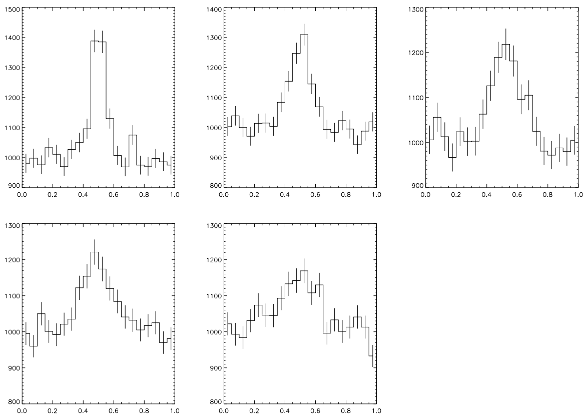

Figure 20: Phase histograms with background counts and pulsed counts fixed, with increasing FWHM.

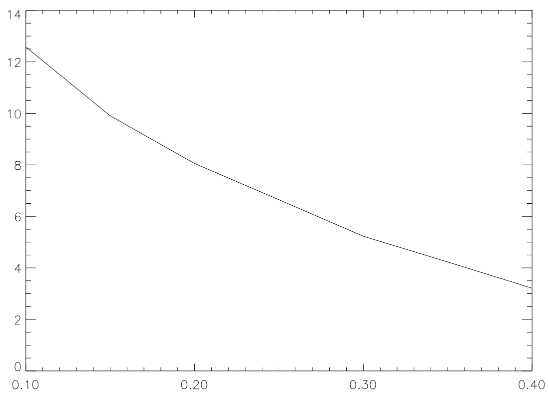

Figure 21: The signal to noise ratio as a function of FWHM of the signal.

4 Dust in Distant Galaxies

4.1 General Cosmology

First we will describe some general theory concerning cosmology. To start with: the universe expands. The recession velocity is proportional to the distance, according to Hubble's Law: $v = H_0 d$, with H_0 Hubble's Constant, which we will take 75 km s^{-1} Mpc^{-1} in this session. This expansion gives rise to a small redshift of the wavelengths in the galaxy light, according to $\Delta\lambda/\lambda = v/c$, the Doppler effect. Hubble's Law implies that at certain distances the velocity of the object exceeds the speed of light. This confusion is solved by realizing that the Doppler effects 'builds' during the travel of the light. While the light travels towards us, space expands and that's what causes the redshift. The relation between wavelength shift and redshift is:

$$z \equiv \frac{\lambda_0 - \lambda_e}{\lambda_e} \tag{11}$$

When calculating flux from luminosity and distance we can no longer use

$$F = L/(4\pi d^2) \tag{12}$$

, but instead we define a 'luminosity distance' d_L, such that

$$F = L/(4\pi d_L^2) \tag{13}$$

At small redshifts, we have $d_L \approx cz/H_0$. At large redshift the relationship gets nonlinear in z. For now we will use a redshift of $z = 1$. For that distances we have

$$d_L = 1.2\Big(\frac{c}{H_0}\Big) \tag{14}$$

Similarly, angular diameter $\delta\theta$ and linear size l are related by

$$\delta\theta = l/d = \frac{H_0 l}{cz} \tag{15}$$

At $z = 1$ we define the 'angular diameter distance' to be

$$d_\theta = 0.3\Big(\frac{c}{H_0}\Big) \tag{16}$$

4.2 Infrared Dust Emission

We will first consider the spectral distribution and flux of the infrared dust emission. Let's assume a galaxy with an intrinsic bolometric luminosity of $10^{11} L_\odot$ at a redshift of $z = 1$. The spectrum of the luminous IRAS galaxies can well be described by blackbodies, with an implied dust temperature of 50 - 100 K. We will take $T_D = 60$ K as a characteristic value. According to the blackbody distribution, from Wiens displacement law($\lambda_{max} T = k_W$), the peak wavelength of the spectrum in the galaxies own rest frame is λ_{max} =48,3 μm. The redshifted spectrum still looks like a blackbody spectrum, and it can be described with a temperature defined by

$$T_D^{'} = T_D/(1+z) \tag{17}$$

because,

$$(1+z) = \frac{\lambda_0}{\lambda_e} = \frac{T_D}{T_D^{'}} \tag{18}$$

The redshifted peak, therefore, has its peak at $\lambda_{max} = 96,6$ μm.

For the assumed intrinsic luminosity of $10^{11} L_\odot$, we calculate the flux on earth, again assuming that the galaxy is at $z = 1$. The flux is: $F = 1.54 \cdot 10^{-27}$ W m^{-2}. A blacbody fairly strongly peaked around λ_{max}, so we can make a rough estimate of the monochromatic energy flux density, F_λ, by using $F_\lambda \approx F/\lambda_{max}$. In our case $F_\lambda = 1.59 \cdot 10^{-29}$ W m^{-2} μm^{-1}.

4.3 Detection of LIG's

To observe Luminous Infrared Galaxies (LIG's) we need to get very high in or above the Earths atmosphere. This is because the atmosphere absorbs all radiation. If we are high enough, our instrument will be able to detect it. Of course there will be a lot of noise. A few sources of noise and background will be the temperature radiation of the instrument itself, the temperature radiation of the vehicle which takes it that high, the temperature radiation of the surrounding and other sources of infrared radiation in the universe, in the line of sight.

If we ignore the instrument contributions and will just be aware of the sky background. We will work out the design parameters for our instrument, assuming we try to detect a $10^{11} L_\odot$ LIG at $z = 1$ that is limited by the sky background. There is a quantity that describes how well (if at all) you can detect a source of radiation, and it is called the Signal to Noise Ratio (SNR). It is defined as:

$$S/N = \frac{N_{source}}{\sqrt{N_{source} + N_{sky}}} \approx \frac{N_{source}}{\sqrt{N_{sky}}} \tag{19}$$

The last approximation can be made because the sky background is stronger than the signal. Some equations we need:

$$\Delta\Omega = \pi(\delta\theta)^2 + \left(\frac{\lambda}{D}\right)^2 \tag{20}$$

$$N_{sky} = \frac{I_{sky} \cdot \pi(D/2)^2 \cdot \Delta\Omega \cdot T_{exposure} \cdot \Delta\lambda}{(h \cdot c)/\lambda} \tag{21}$$

$$N_{source} = \frac{1}{2}(S/N)^2 + \sqrt{(S/N)^4 + 4(S/N)^2 \cdot N_{sky}} \tag{22}$$

Using expressions given above we calculate the apparent size of the galaxy on the sky if its real diameter is 20 kpc: $\delta\theta = 3.4$ arcseconds. The radius projected is therefore $\delta\theta = 1,'' 7$.

We are now able to write down an expression for the faintest flux we can still detect above the sky background:

$$F_{min} = \frac{N_{source}}{\pi(D/2)^2 \cdot T_{exp} \cdot \Delta\lambda} \tag{23}$$

Now it turns out to be convenient to make a plot of the limiting flux curve. We choose our telescope diameter as the independent variable, and we plot the limiting flux as a function of it. The plot can be seen in Figure 22.

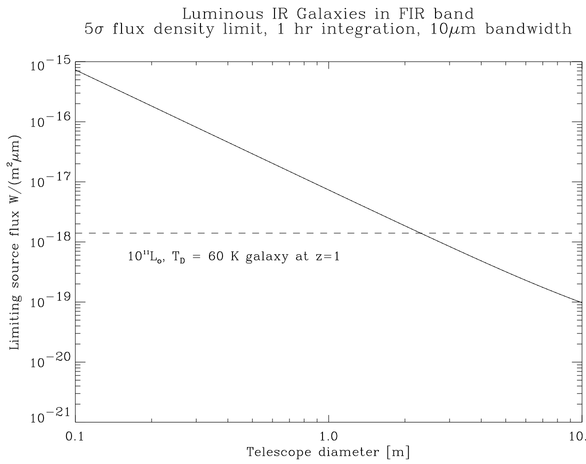

Figure 22: The limiting flux as a function of telescope diameter.

From this plot we conclude that our telescope must be at least approximately 2.5 meters to detect our galaxy.